Application of magnetorheological elastomer to vibration absorber

Hua-xia Deng, Xing-long Gong *

CAS Key Laboratory of Mechanical Behavior and Design of Materials, Department of Mechanics and Mechanical Engineering, University of Science and Technology of China, Hefei 230027, China

Abstract

Traditional dynamic vibration absorber (DVA) is widely used in industries as a vibration absorption equipment. However, it is only effective at narrow working frequency range. This shortcoming has limited its stability and application. This paper develops an adaptive tuned vibration absorber (ATVA) based on unique characteristics of magnetorheological elastomers (MREs), whose modulus can be controlled by an applied magnetic field. This ATVA works in shear mode and consists of dynamic mass, static mass and smart spring elements with MREs. Based on the double pole model of MR effects, the shift-frequency capability of the ATVA has been theoretically and experimentally evaluated. The experimental results demonstrated that the natural frequency of the ATVA can be tuned from 27.5 Hz to 40 Hz. To study its vibration absorption capacity, a beam structure with two ends supported has been employed. To analyze the vibration absorption capacity, a dynamic model of coupling beam and absorber has been established. Both the calculation and experimental results show that the absorption capacity of the developed ATVA is better than the traditional TVA and can achieve as high as 25 dB which was justified by the experiment.
© 2007 Elsevier B.V. All rights reserved.

PACS: 70.10.Fq

Keywords: Magnetorheological elastomer (MRE); Adaptive tuned vibration absorber (ATVA); Vibration control

1. Introduction

Magnetorheological (MR) materials are smart materials which have MR effects and many unique properties with magnetic field. MR effect is that the rheological properties will change under applied magnetic field. Since its first discovery by Rabinow at 1948 [1], MR materials have developed into a family with MR fluids, MR foams and MR elastomers [2]. The most common MR material is MR fluids (MRFs) which are suspensions of magnetically polarizable particles in viscous fluids [3]. The general criterion to estimate the MR effect of MRFs is the variation capability of dynamic yield stress within a post-yield regime under applied magnetic field.

---

* Corresponding author. Tel./fax: +86 551 3600419.
  E-mail address: gongxl@ustc.edu.cn (X.-l. Gong).

Numerous applications based on MRFs benefit from the properties that the dynamic yield stress can be continuously, rapidly and reversibly controlled by the applied magnetic field. Such applications have been applied on varies of fields such as automotive industry [4–6], earthquake-resistance [7] and vibration control [8] and have been commercialization and industrialization. For instance, the LORD Corporation of American has professionally applied itself to researching, manufacturing, distributing MRFs and series of applications based on these materials such as brakes, clutches and variable-friction dampers. But MRFs also exhibit some shortcomings which hinder in the applications such as deposition, environmental contamination [9] and sealing problems.

MR elastomers (MREs), the structural solid analogues of MRFs may be a good solution to overcome these disadvantages. MREs are composed of polarizable particles dispersed in a polymer medium. Typically, magnetic fields are applied to the polymer composite during crosslinking so that particles form chainlike or columnar structures, which are fixed in the matrix after curing [10]. The comparison of MREs and MRFs is that the MR effect of MREs is the field-dependent modulus with in pre-yield regime [11]. Such properties stimulate their many promising applications such as adaptive tuned vibration absorbers (TVAs), stiffness tunable mounts and suspensions, and variable impedance surfaces. Compared with MRFs, the application of MREs is still at exploring stage. Watson [12] applied an patent using MREs, method and apparatus for varying the stiffness of a suspension bushing; Ginder et al. [13,14] constructed and tested tunable automotive mounts and bushings based on MR elastomers which can be applied to minimize the effect of suspension resonances excited by torque variation due to worn brake rotors by shifting the resonance away from the excitation frequency. Ginder and coworkers [15] did pioneer work on the development of an adaptive tunable vibration absorber (ATVA) using MREs. Their initial experimental results indicated that the ATVA had the capability to shift frequency from 500 Hz to 610 Hz.

Traditional dynamic vibration absorber (DVA) theoretically brings the object base to rest at a single excitation frequency, the resonance frequency of the DVA. It means that the absorber is usually used to suppress a single harmonic excitation of the vibrating systems. For many practical systems, which have time-varying vibration sources or wide vibration frequency bandwidth, the passive absorber will lose its effect and potentially aggravate the base vibration. After prototype of ATVA using MRE as an adaptive tuned element has been succeeded by our group [16], a shear mode vibration absorber which is more compact and more utilizable was developed in this paper. The objective of this paper is to investigate the frequency-shift property and vibration absorption capability of the developed ATVA. To this goal, an experimental system is set up to evaluate the ATVA and a simple theoretic analysis is developed to confirm the observed frequency-shift property. Further more, a dynamic model is established to simulate the vibration absorption capability of the developed ATVA and predict a good future of this ATVA.

2. ATVA design

2.1. Material preparation

The MRE materials consist of 704 silicone rubbers as a matrix, carbonyl iron particles with size of 3–5 μm, and a small amount of silicone oil. The schematic diagram of the fabrication method is shown in Fig. 1. At the first step of the fabricating process, all ingredients are thoroughly blended with an agitator. Then the mixture is packed into an aluminum mold and placed in the vacuum to take out the air in the mixture. After that, seal the mold and place it in a magnetic field of 1 T for 24 h. Particles will be arranged in chain formation resulted from the anisotropic magnetic forces among the particles. When the elastomer is cured, such ordered structure is locked in the matrix.

2.2. MRE characterization

Fig. 2 is a photograph of the MRE testing system, which is modified by our group on the base of the Dynamic mechanical analyzer (DMA) system from the Triton Co. (model: tritec2000). To measure MRE properties under various magnetic fields, an electromagnet was developed, which can provide magnetic field intensity up to 1100 mT. With this system, both the shear modulus and the loss factor against magnetic field at various excitation frequencies were measured. The results are shown in Fig. 3. It can be seen from Fig. 3a that
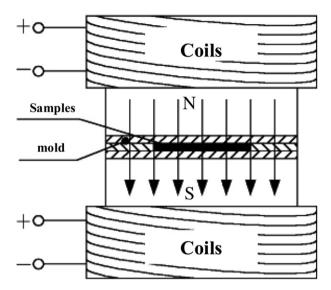
Fig. 1. The schematic diagram of the fabrication method.

Fig. 2. Photograph of the modified DMA.

the shear modulus shows an increasing trend with magnetic field intensity. However, the increasing slope decreases with the increment of magnetic fields, which is due to the magnetic saturation. In addition, the modulus also shows an increasing trend with loading frequency, which justifies that MRE performs viscoelastic behavior. Fig. 3b shows the loss factor is independent of magnetic field and frequency, which was reported before [17].

2.3. ATVA structure

The core of this design is to utilize the limit space as efficiently as possible. The efficient component for ATVA to vibration absorption is its oscillator or a dynamic mass. The schematic diagram of the developed ATVA is shown in Fig. 4. As shown in this figure, the ATVA consists of three main parts: dynamic mass, static mass and smart spring element with MREs. The electromagnets and magnetic conductors form a closed C-shape magnetic circulate, which are assembled at mounting shell to be the dynamic mass. This development makes the ATVA more compact and more efficient because no additional oscillator and nearly most
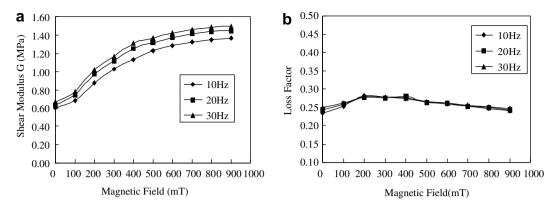
Fig. 3. Variation of shear modulus and loss factor with magnetic field at different loading frequency (a) magnetic field (mT) (b) magnetic field (mT).
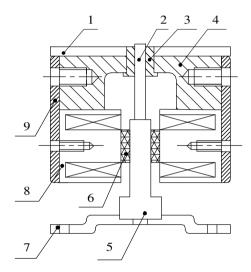

Fig. 4. The schematic diagram of the developed ATVA: 1. cover; 2. guiderod; 3. linear bearing; 4. magnetic conductor; 5. shear plate; 6. MREs; 7. base; 8. electromagnet; 9. mounting shell.

components were moved to be dynamic mass. The static mass consists of the shear plate and the base. Through the shear plate, MREs which are tested above connect the dynamic mass and the static mass. To ensure the ATVA works in the shear mode, a guiderod and a linear bearing are employed.

The working principle of the system is as below. The magnetic field is created by two coils in the electromagnets and the field strength is controlled by the coil current, provided by an external DC power. As MRE's shear modulus depends on the field strength, the equivalent stiffness of the ATVA changes with the field strength as well as the coil current. Consequently, the natural frequency of the ATVA can be controlled by the coil current. Thus, the ATVA natural frequency can be changed by tuning the coil current to trace the external excitation frequency. When the tuned ATVA frequency matches the excitation frequency, the vibration can be attenuated significantly. This point will be theoretically addressed in the following section.

3. ATVA testing

3.1. Experimental study of frequency-shift property

For simplicity, a beam with both ends supported is employed to investigate the frequency-shift capability of the MREs. The experimental setup is shown in Fig. 5. The beam is made up of low carbon steel, with the size
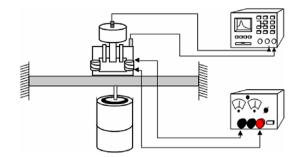
Fig. 5. The evaluation system of frequency-shift property.

of 930 mm × 100 mm × 11 mm. The material parameters are: Young's modulus $E = 200$ GPa, density $\rho = 7800$ kg/m^3, Poisson's ratio $v = 0.3$, and the loss factor $\eta = 0.05$. Using the modal analysis, its first and second mode natural frequencies are 60 Hz, and 250 Hz, respectively. As shown in Fig. 5, the experimental procedure is as below. The developed ATVA is placed at the centre of the beam. White noise excitation applied to the beam is generated by an exciter (model: JZK-10, manufactured by Sinocera Piezotronics INC., China). Two accelerometers (model: PCB 3510A) are placed on the oscillator and the base beam to measure their responses, respectively. The measured signals are sent to the Dynamic Signal Analyzer (model: Signal Calc ACE DP240, Data Physics Corp.). The transfer function can be obtained by using FFT analysis. The frequency-shift capability at various magnetic fields of the ATVA based on MREs is shown in Figs. 6 and 7. The two figures show that the magnitude curve and the phase curve of transfer function moves rightward with the increase of the magnetic field. The resonance frequency can be obtained by reading the peak-to-peak value or the frequency at 90degr at the phase curve. By tuning the coil current, the relationship of the resonance frequency of the absorber versus the coil current can be obtained and it is shown in Fig. 8. The
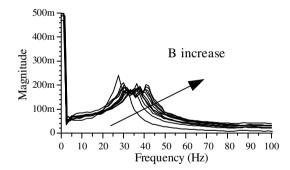

Fig. 6. The magnitude curve versus frequency at various magnetic fields.
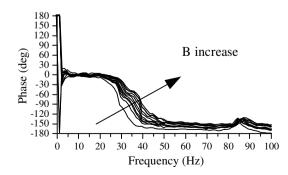

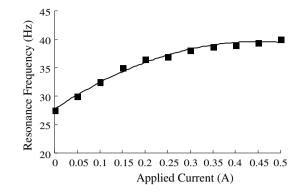Fig. 7. The phase curve versus frequency at various magnetic fields.

Fig. 8. The relationship between applied current and resonance frequency.

resonance frequency increases from 27.5 Hz at 0 A to 40 Hz at 0.5 A. Its relative frequency change is as high as 145%.

3.2. Theoretic analysis of frequency-shift property

The resonance frequency of the TVA is represented as

$$f = \frac{1}{2\pi}\sqrt{\frac{k_\tau}{m}}, \tag{1}$$

where m is the mass of oscillator, k_τ is the equivalent shear stiffness.

In the shear direction, k_τ is given by

$$K_\tau = \frac{GA}{h}, \tag{2}$$

where G is MRE's shear modulus, A is the shear area, and h is the thickness of MREs.

The MRE shear modulus G consists of two terms, as below

$$G = G_0 + \Delta G_d, \tag{3}$$

where G_0 is the initial shear modulus without any magnetic field, ΔG_d is the shear modulus increment under the applied magnetic field. The double pole model is widely used to predict the magnetic induced shear modulus increment [18]. Using this model, the shear modulus increment under the magnetic field is given by [19]

$$\Delta G_d = 36\phi\mu_f\mu_0\beta^2 H_0^2 \left(\frac{R}{d}\right)^3 \zeta, \tag{4}$$

where $\beta = (\mu_p - \mu_f)/(\mu_p + 2\mu_f) \approx 1$, μ_0 is the vacuum permeability, $\mu_p \approx 1000$ and $\mu_f \approx 1$ are relative permeability of particles and silicon rubber matrix, respectively. ϕ is volume fraction, R is the average particle radius, d is the particle distance before deflection, H_0 is the applied magnetic field intensity, and $\zeta = \sum_{k=1}^{\infty} 1/k^3 \approx 1.202$. When the magnetic field is high enough, some particles will saturate, Eq. (4) is not long valid. When all particle saturate, Eq. (4) will be replaced as

$$\Delta G_d = 4\phi\mu_f\mu_0 M_s^2 \left(\frac{R}{d}\right)^3, \tag{5}$$

where M_s is particle's saturation intensity.

Substituting Eqs. (2) and (3) into Eq. (1), the natural frequency is rewritten as

$$f = f_0 + \Delta f, \tag{6}$$

where f_0 is the resonant frequency without magnetic field, Δf is the shift of resonance frequency due to the applied magnetic field

$$f_0 = \frac{1}{2\pi}\sqrt{\frac{G_0 A}{mh}}, \tag{7}$$

$$\Delta f = \frac{1}{2\pi}\sqrt{\frac{G_0 \times A}{m \times h}} \cdot \left(\sqrt{1 + \frac{\Delta G_d}{G_0}} - 1 \right). \tag{8}$$

From the Eq. (7), the initial resonant frequency of the ATVA can be designed to match the vibration system, the focus of the vibration attenuation. Eq. (8) reveals that the frequency-shift capacity is not only proportional with the MR effect but also relative to the initial shear modulus. The larger initial modulus with the same MR effect will cause the wider frequency-shift bandwidth. When $\Delta G_d \ll G_0$, Eq. (8) can be approximately substituted by Eq. (9)

$$\Delta f = \frac{\Delta G_d}{4\pi}\sqrt{\frac{A}{G_0 mh}}. \tag{9}$$

The frequency-shift is proportional to the shear modulus increases, and it can be seen from the beginning of the curve shown in Fig. 8.

When ΔG_d is as large as G_0, Eq. (9) is not valid. Substituting Eq. (4) into Eq. (7), the frequency-shift can be rewritten as below:

$$\Delta f = \frac{1}{2\pi}\sqrt{\frac{G_0 \times A}{m \times h}} \cdot \left(\sqrt{1 + \frac{36\phi\mu_f\mu_0\beta^2 H_0^2 (\frac{R}{d})^3 \zeta}{G_0}} - 1 \right). \tag{10}$$

Similarly, substituting Eq. (5) into Eq. (7), the frequency-shift at saturation status is a constant as given by

$$\Delta f = \frac{1}{2\pi}\sqrt{\frac{G_0 \times A}{m \times h}} \cdot \left(\sqrt{1 + \frac{4\phi\mu_f\mu_0 M_s^2 (\frac{R}{d})^3}{G_0}} - 1 \right). \tag{11}$$

The theoretical trend presented by Eqs. (9)–(11) agrees well with the results shown in Fig. 8 qualitatively.

3.3. The study on vibration attenuation

The effect of vibration absorption can be evaluated by the system shown in Fig. 9. Compared with the frequency-shift experiment, the major difference is that an impedance head is induced. As shown in this figure, the impedance head connects with the beam and the exciter. The exciter provides sinusoidal excitation to the beam with a linear frequency scan from low to high. The natural frequency will be tuned by changing coil current to trace the excitation frequency. The base point impedance with various magnetic fields can be measured by the dynamic signal analyzer. If the magnetic field is fixed, the absorber can be looked as a classical
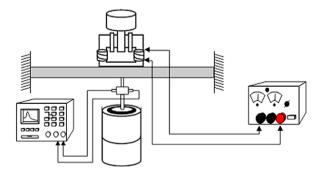

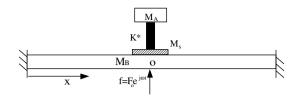Fig. 9. The evaluation system for vibration attenuation.

Fig. 10. The simplification model of evaluation system.

passive TVA with fixed resonance frequency. To evaluate the vibration absorption capacity, a ratio γ of base point admittance with TVA and without TVA is employed.

The system in Fig. 9 can be simplified as shown in Fig. 10. Suppose the force and velocity applied to the base point O is F_0, and V_0, respectively. The resultant forces and velocities at the lower and upper points of the static mass M_s are F_s^b, V_s^b and F_s^t, V_s^t, respectively. The resultant force and velocity of the absorber mass M_A are F_A and V_A. The admittance at point O is defined as H_0^b and given by

$$H_0^b = \frac{V_0}{F_0} = \frac{\mathrm{j}\omega}{M_B} \sum_{k=1}^{n} \frac{\phi_k^2(x_0)}{\omega_k^2(1+\mathrm{j}\eta) - \omega^2}, \tag{12}$$

where ω_k and ϕ_k are the kth natural frequency and mode function, x_0 is the coordinator of the point O, n is the mode number, η is the loss factor, ω is the excitation frequency, $\mathrm{j} = \sqrt{-1}$. Eq. (12) can be simplified as

$$V_0 = \frac{\Delta H}{H_0^b + \Delta H} H_0^b F_0, \quad \Delta H = 1 \Big/ \left(\mathrm{j}\omega M_s + \frac{\mathrm{j}\omega M_A K^*}{K^* - \omega^2 M_A} \right), \tag{13}$$

where ΔH is the additional admittance at the point O due to the absorber and the mass, K^* is the complex stiffness of absorber, The complex stiffness can be expressed by conventional spring's stiffness K, damping factor C and damping ratio ξ:

$$K^* = K(1 + \mathrm{j}\omega C/K) = K(1 + 2\mathrm{j}\omega\omega_0\xi M_A/K). \tag{14}$$

The admittance at the point O with absorber is given by

$$H_A = \frac{\Delta H}{H_0^b + \Delta H} H_0^b. \tag{15}$$

When there is no active mass, the admittance at the point O is given by

$$H_0 = \frac{\Delta H^s}{H_0^b + \Delta H^s} H_0^b, \quad \Delta H^s = 1/(\mathrm{j}\omega M_s). \tag{16}$$

The ratio γ to reflect the effect of vibration absorption capacity can be defined as

$$\gamma = 20 lg(|H_A/H_O|). \tag{17}$$

The comparison of vibration absorption capacity which is apart from the natural frequency of the primary system between the adaptive TVA and the passive one is shown in Fig. 11, where the upper data are the results of passive TVA whose resonance frequency is fixed at 35 Hz and the lower data are the results of ATVA whose frequency is tuned to trace the excitation frequency. As shown in Fig. 11, experimental data and numerical curve are very close. It indicates that the dynamic model is reasonable and the experimental data is reliable. For the passive TVA, the best vibration attenuation efficiency occurs at the natural frequency of the primary system. The effect become worse sharply while the excitation frequency is apart from beam natural frequency and a new resonance hump occurs at 27 Hz. For ATVA, limited to the MR effect of spring element, ATVA can not be experimentally evaluated at the entire frequency band. In tunable frequency band, the comparison between adaptive TVA and passive one indicates that ATVA has better absorbing effects than passive TVA. For example, at 40 Hz, the ATVA's effect of vibration absorption is −22 dB while it is −8 dB for the passive TVA. For even wider bandwidth, theoretical analysis which is shown at Fig. 12 predicts that the ATVA also has better effects and there is no resonance hump at the formant frequency of the passive TVA.
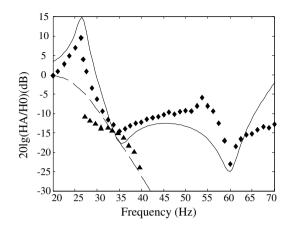
Fig. 11. comparison of vibration attenuation between ATVA and TVA: (▲) adaptive (experimental data); (♦) passive (experimental data); (---) adaptive (numerical data); (—) passive (numerical data).
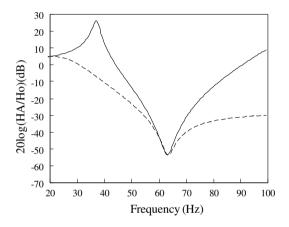

Fig. 12. The theoretical calculation of the vibration attenuation: (---) adaptive (numerical data); (—) passive (numerical data).

4. Conclusion

A shear mode ATVA with MRE was developed in this paper. It consists of dynamic mass, static mass and smart spring elements with MREs. Both theoretical and experimental results indicate that the resonance frequency of the developed ATVA can be controlled by electrical currents. The resonance frequency varies from 27.5 Hz at 0 A to 40 Hz at 0.5 A. Its relative frequency change is as high as 145%. To evaluate the vibration absorption capability of TVA, a beam with two ends supported is used as an object base and the ratio γ of base point admittance with TVA and without TVA is employed. The experimental results agree well with theoretical calculation and they all demonstrate that the developed ATVA has better performance than conventional passive absorber in terms of frequency-shift property and vibration absorption capacity.

Acknowledgements

References

[1] Rabinow J. The magnetic fluid clutch. AIEE Trans 1948;67:1308–15.

[2] David CJ, Jolly MR. MR fluid, foam and elastomer devices. Mechatronics 2000;10:555–69.

[3] Zhang XZ, Gong XL, Zhang PQ, Wang QM. Research on mechanism of squeeze-strengthen effect in magnetorheological fluids. J Appl Phys 2004;96:2359–64.

[4] Phule PP, Ginder JM. Synthesis and properties of novel magnetorheological fluids having improved stability and redispersibility. Int J Mod Phys B 1999;13(14-16):2019–27.

[5] Ginder JM. Behavior of magnetorheological fluids. MRS Bull 1998;23(8):26–9.

[6] Ginder JM, Davis LC, Elie LD. Rheology of magnetorheological fluids: models and measurements. Int J Mod Phy B 1996;10(23–24):3293–303.

[7] Dyke SJ, Spencer BF, Sain MK, Carlson JD. An experimental study of MR dampers for seismic protection. Smart Mater Struct 1998;7(5):693–703.

[8] Jung HJ, Spencer BF, Lee IW. Control of seismically excited cable-stayed bridge employing magnetorheological fluid dampers. J Struct Eng—ASCE 2003;129(7):873–83.

[9] Shen Y, Golnarghi MF, Heppler GR. Experimental research and modeling of magnetorheological elastomers. J Intell Mater Syst Struct 2004;15:27–35.

[10] Wang YL, Hu Y, Gong XL, Jiang WQ, Zhang PQ, Chen ZY. Preparation and properties of magnetorheological elastomers based on silicon rubber/polystyrene blend matrix. J Appl Polym Sci 2007;103(5):3143–9.

[11] Zhou GY. Shear properties of a magnetorheological elastomer. Smart Mater Struct 2003;12:139–46.

[12] Watson JR, Canton Mich. Method and apparatus for varying the stiffness of a suspension bushing. US Patent 5,609,353; 1997.

[13] Stewart WM, Ginder JM, Elie LD, Nichols ME. Method and apparatus for reducing brake shudder. US Patent 5,816,587; 1998.

[14] Ginder JM, Nichols ME, et al. Controllable-stiffness components based on magnetorheological elastomers. Proc SPIE 2000;3985:418–25.

[15] Ginder JM, Schlotter WF, Nichols ME. Magnetorheological elastomers in tunable vibration absorbers. Proc SPIE 2001;4331:103–10.

[16] Deng HX, Gong XL, Wang LH. Development of an adaptive tuned vibration absorber with magnetorheological elastomer. Smart Mater Struct 2006;15:111–6.

[17] Gong XL, Zhang XZ, Zhang PQ. Fabrication and characterization of isotropic magnetorheological elastomers. Polym Test 2005;24(5):669–76.

[18] Shiga T, Okada A, Kurauchi T. Magnetoviscoelastic behavior of composite gels. J Appl Polym Sci 1995;58:787–92.

[19] Davis LC. Model of magnetorheological elastomers. J Appl Phys 1999;85:3348–51.